

Supporting Information

Carbon Nanotubes-Stabilized Co₉S₈ Dual-Shelled Hollow Spheres for High-performance K-ion Storage

Jie Zhou,^a Haoyu Zhao,^a Qianliang Zhang,^b Tieqiang Li,^a Yang Li,^a Ning Lin*,^a Yitai Qian^{ab}

a. Hefei National Laboratory for Physical Science at Micro-scale, Department of Chemistry, University of Science and Technology of China, Hefei, Anhui 230026, P. R. China. E-mail: ningl@mail.ustc.edu.cn.

b. School of Chemistry and Chemical Engineering, Shandong University, Jinan, Shandong 250100, P. R. China.

1. Experimental section:

1.1 Materials. Co(NO₃)₂•6H₂O, thioacetamide (TAA), sublimed sulfur, glycerol, isopropanol and ethanol were purchased from Sinopharm Chemical Reagent Co., Ltd. (China). All the chemical reagents used here were analytical grade without further purification.

1.2 Synthesis of double-shelled hollow Co₉S₈ nanospheres and Co₉S₈/CNTs composites. In a typical process, 218 mg Co(NO₃)₂•6H₂O and 8 ml glycerol were dissolved in 40 ml isopropanol. After 20 min stirring, the transparent pink solution was then sealed in a Teflon-lined stainless-steel autoclave and heated at 180 °C for 6 h. As the autoclave cooled down to room temperature, the light pink precipitate was collected by centrifugation and washed with ethanol several times. After dried in the

oven at 60 °C, 30 mg of the obtained precursor Co-glycerate spheres and 75 mg TAA were added into 20 mL ethanol, stirred for 2 h and transferred into Teflon-lined stainless-steel autoclave. After heating at 160 °C for 6 h, the black product was obtained by centrifugation, washed with ethanol several times and finally dried in the vacuum oven at 60 °C. In the solvothermal condition, sulfide (S^{2-}) ions released from the decomposition of TAA reacts with the metal ion in Co-glycerate sphere which is called the sulfidation process. The S^{2-} diffuses inwards and the metal ion diffuses faster outwards, which results in the formation of core-shell structure. As the time goes on, the gap between core and shell becomes large. It is difficult for the metal ion to continue to diffuse outward. The second shell will form in the remaining core with the similar process as the formation of the outer-shell. After a certain time, the double-shell hollow spheres are obtained. For the preparation of double-shelled Co_9S_8 nanospheres, the as-prepared samples were annealed at 500 °C under the Ar atmosphere for 6 h. For the preparation of Co_9S_8 /CNTs composites, the as-prepared samples were annealed at 500 °C under the continuous acetylene/argon gas flow (1/9) for 6 h.

1.3 Materials characterization. The structure and morphology of the product were characterized by X-ray diffractometer (Philips X'Pert Super diffract meter with $Cu\ K\alpha$ radiation ($\lambda=1.54178\ \text{\AA}$)), Raman spectrometer (Lab-RAM HR UV/VIS/NIR), X-ray photoelectron spectroscopy (XPS) (ESCA-Lab MKII X-ray photoelectron spectrometer), scanning electron microscopy (SEM, JEOL-JSM-6700F), and transmission electron microscopy (TEM, Hitachi H7650 and HRTEM, JEOL 2010),

the BET (Brunauer-Emmett-Teller) surface areas and the BJH (Barrett-Joyner-Halenda) pore distribution calculated by the Nitrogen adsorption-desorption method (ASAP 2020 M+C, Micromeritics), Thermogravimetric analysis (TGA, DTG860H Shimadzu).

1.4 Electrochemical measurement.

The K-storage performances of the samples were tested with CR2016 coin cells, in which Potassium foils was used as the counter/reference electrode, the electrolyte for PIBs was KPF6 (0.6 mol L⁻¹) in an EC/DEC solution (1:1, v/v). All half-cells were carefully assembled in the Ar-filled glove box (H₂O, O₂ < 0.1 ppm). The anode slurry was fabricated by mixing 60% active materials, 20% super P, 20% sodium alginate (SA) binder in water solvent. The slurry was further coated on one side of the Cu foil and then dried in a vacuum oven at 80 °C for 10 h. After that, the Cu foil was pressed by rolling and cut into a wafer with the diameter of 12 mm. The loading of active material was determined to be about 1.0 mg cm⁻². The cells were galvanostatic discharge/charge under the voltage between 0.01 V and 3.0 V versus K⁺/K at the current density rate of 0.1-5.0 A g⁻¹ using a LAND8CT2001A instrument. The initial coulombic efficiency is further improved via prepotassiate (putting the CS-CNTs electrode in contact with potassium before assembling battery). Cyclic voltammetry (CV) was performed with the CHI660E electrochemical workstation.

The peak current (*i_p*, mA) obeys a power-law relationship with the sweep rate (*v*, mV/s): $i = a v^b$, where *a* and *b* are adjustable values; *b* = 0.5 indicates a semi-infinite diffusion process, and *b* = 1 indicates a capacitive process. A linear relation between

log(scan rate) and log(peak current) can be depicted on basis of the results of cyclic voltammograms.

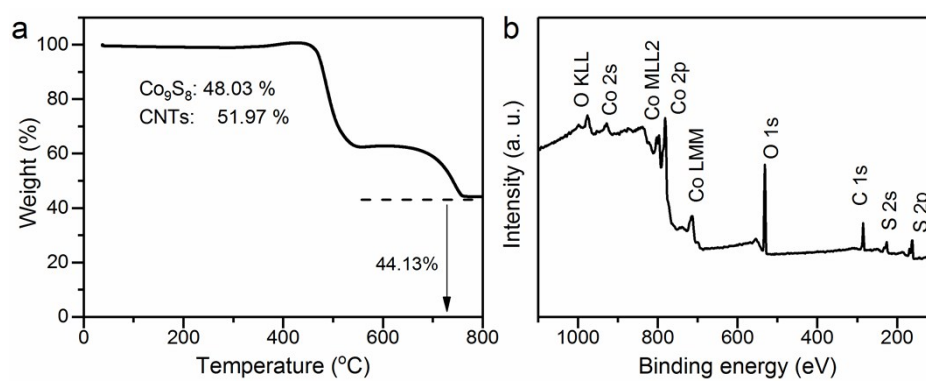


Fig. S1 (a) TGA curve of the CS-CNTs. (b) Survey XPS spectra of CS-CNTs composite.

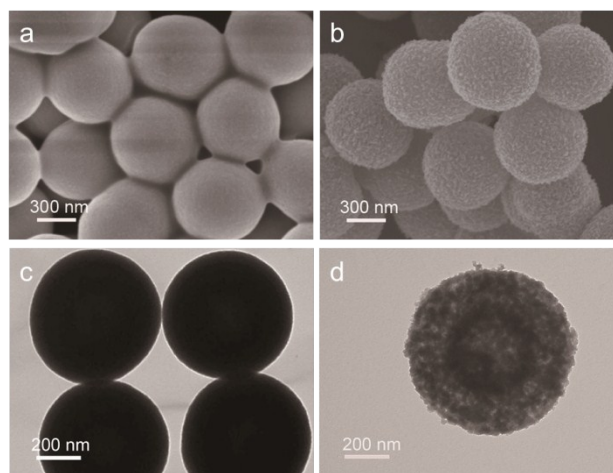


Fig. S2 SEM images of (a) Co-glycerate solid sphere (b) CoS_x double-shells hollow sphere and TEM images of (c) Co-glycerate solid sphere (d) CoS_x double-shells hollow sphere

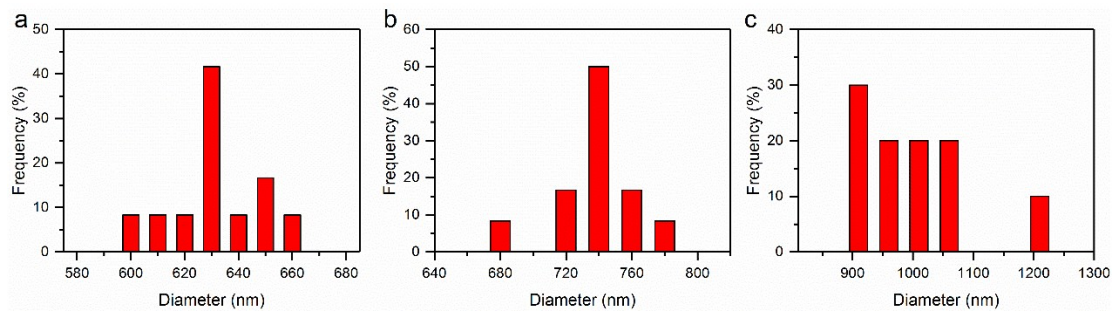


Fig. S3 The particles distribution of (a) Co-glycerate, (b) Co-S precursor, (c) CS-CNTs composite.

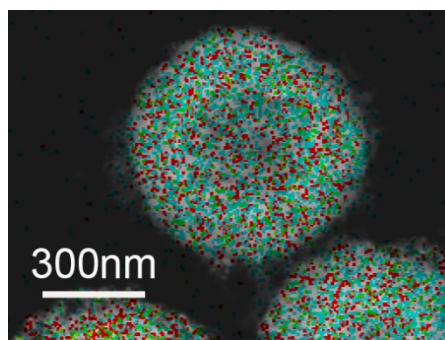


Fig. S4 The HAADF-STEM image and element mapping of CS-CNTs composite.

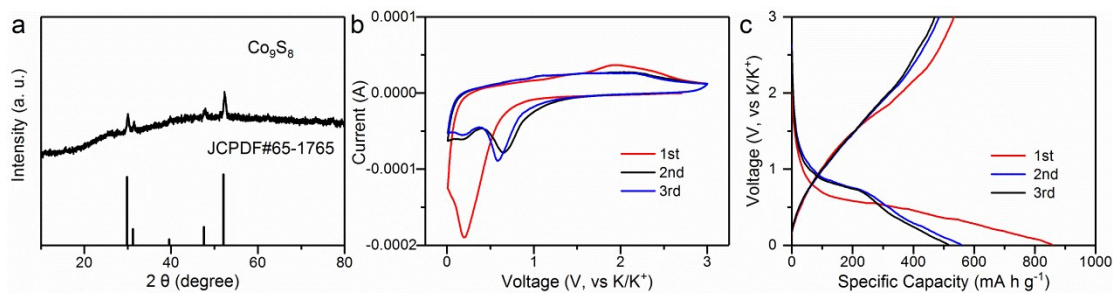


Fig. S5 (a) XRD pattern (b) CV curves and (c) discharge/charge voltage profiles of the CS based electrode.

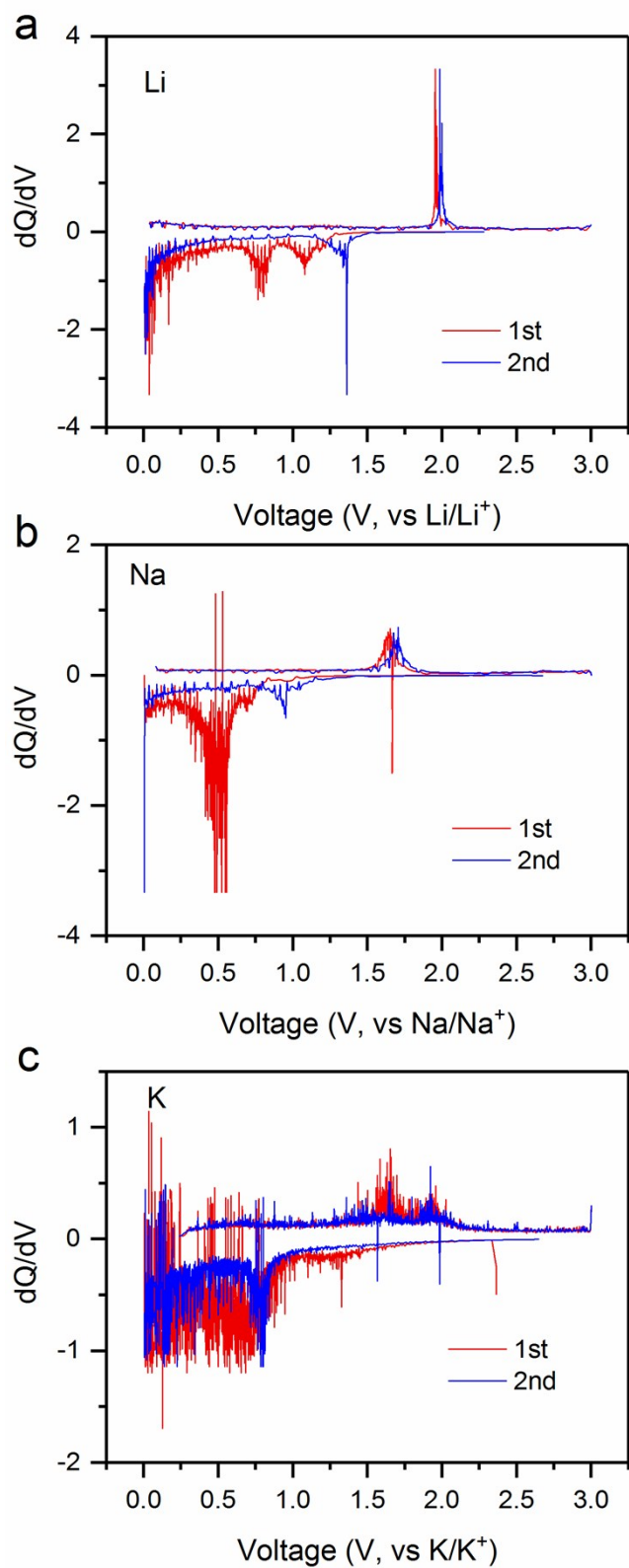


Fig. S6 The dQ/dV plots of CS-CNTs electrode in (a) Li-ion batteries, (b) Na-ion batteries, (c) K-ion batteries.

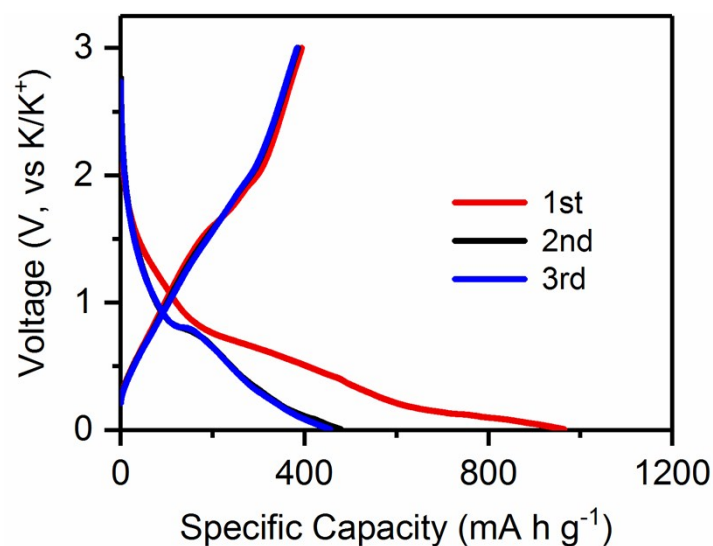


Fig. S7 Galvanostatic charge/discharge curves of CS-CNTs at a constant current of 0.1 A g^{-1} in the voltage window $0.005\text{-}3 \text{ V}$.

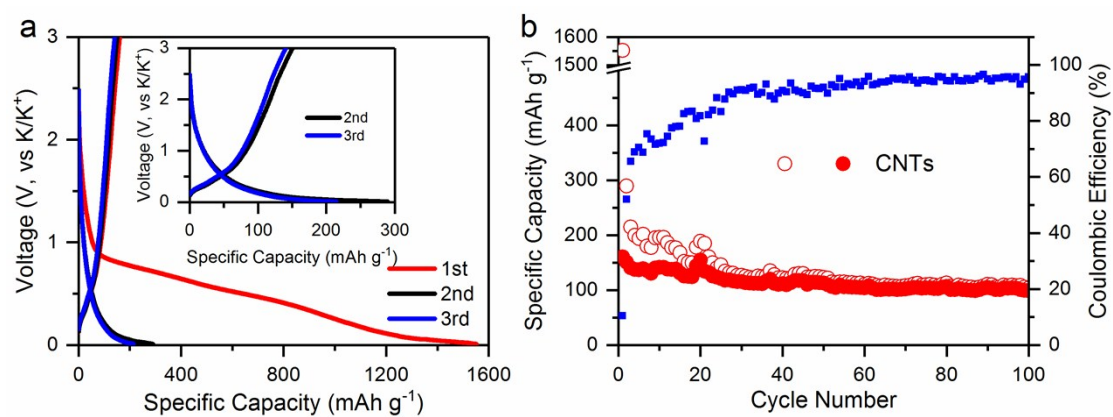


Fig. S8 (a) Galvanostatic charge/discharge curves of CNTs at a constant current of 0.1 A g^{-1} in the voltage window $0.005\text{-}3 \text{ V}$. (b) cycling test at the current of 0.1 A g^{-1} .

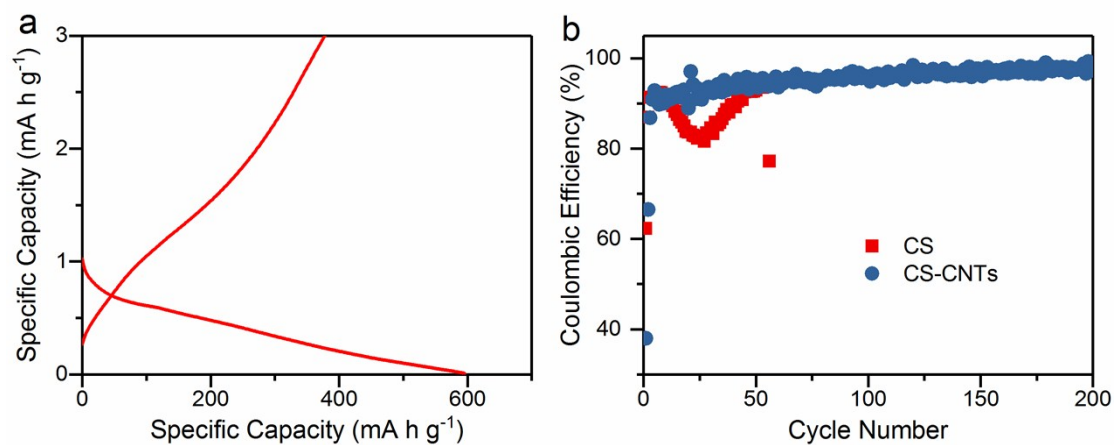


Fig. S9 (a) The Galvanostatic charge/discharge curves of CS-CNTs at a constant current of 0.1 A g^{-1} after prepotassiate. (b) The coulombic efficiency of the CS-CNTs and CS electrodes at a current density of 50 mA g^{-1} .

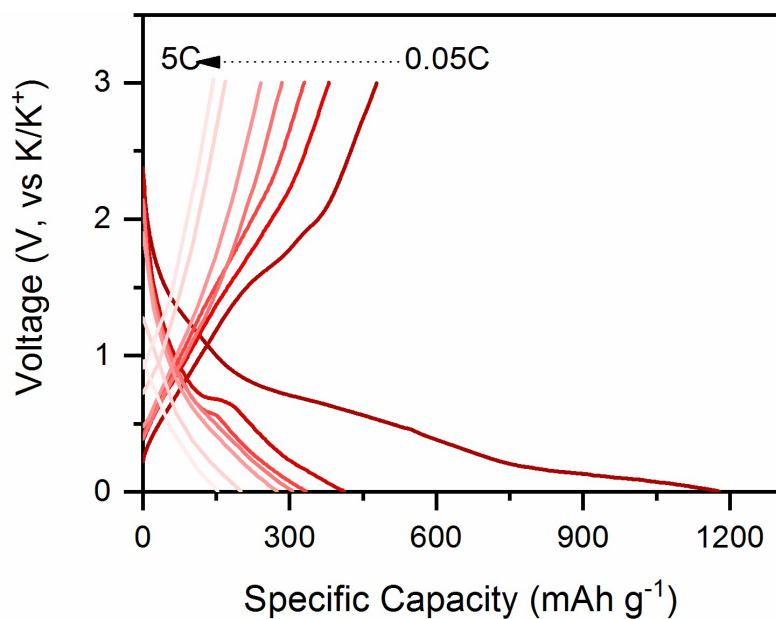


Fig. S10 The discharge/charge capacity-voltage profiles of CS-CNTs electrode at different rates.

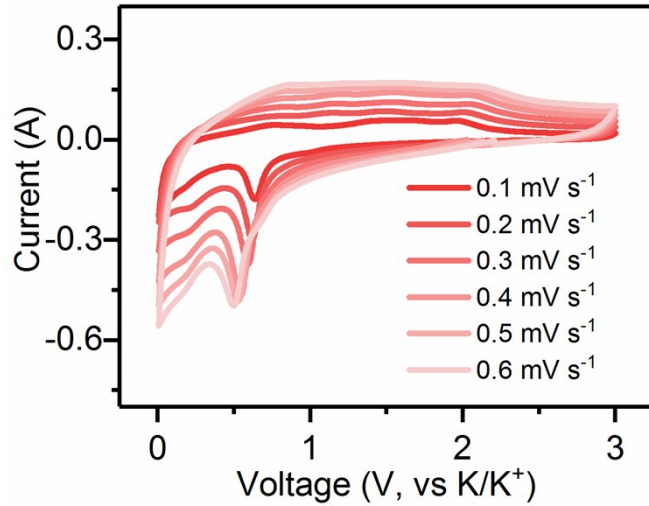


Fig. S11 CV curves at different sweep rates (0.1-0.6 mV s^{-1}) of CS-CNTs

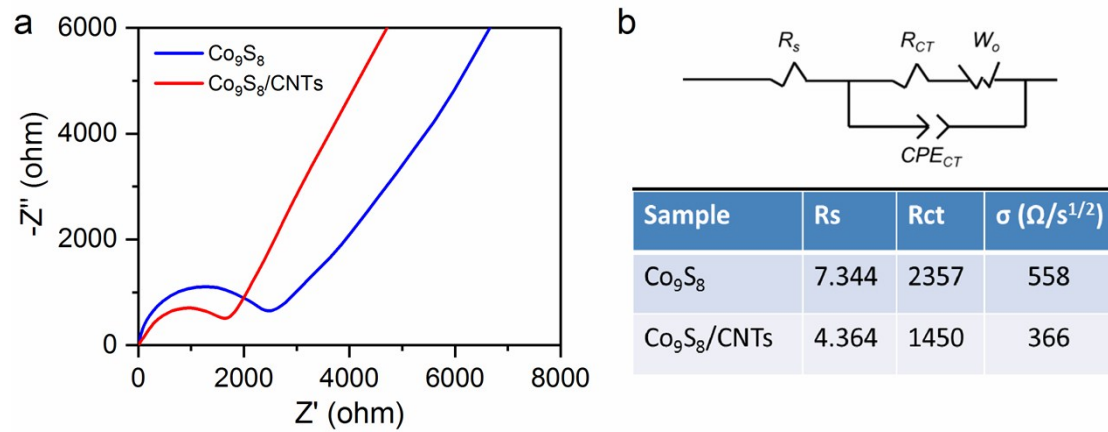


Fig. S12 (a) The Nyquist plots for the EIS data. (b) The corresponding equivalent circuit.

Fig. S12 shows the Nyquist plot of fresh CS-CNTs and CS electrodes. The depressed semicircle and a sloped line are corresponding to the interphase electronic contact resistance in the electrode/electrolyte interface (R_{ct}), and the impedance of lithium-ions diffusion in the bulk electrode. The obvious contrast indicates that the CNTs layer is beneficial to reduce the interface resistance and enhance ionic-diffusion.